Advancing Our Understanding on Ionospheric Threats to SBAS/GBAS Operations Over North and South America

Rezy Pradipta and Patricia H. Doherty

Abstract – We present an overview of our investigation on ionospheric threats to space-based augmentation systems (SBAS) and ground-based augmentation systems (GBAS) over North and South America during solar cycle 24. Overall reductions in the localizer performance with vertical guidance (LPV) coverage area of the Wide Area Augmentation System (WAAS) over North America were identified during geomagnetically disturbed periods. Meanwhile, magnitudes of gradients in total electron content (TEC) over the Brazilian airspace were found to follow a double-power-law distribution. The exponents of this power law were found to vary systematically with sunspot number, causing the tail of the distribution to extend further during the solar maximum, resulting in more frequent occurrence of extreme ionospheric TEC gradients. These circumstances point to the need for civil aviation authorities to receive better information regarding equatorial plasma bubble (EPB) occurrence patterns, both as a function of season and as a function of geomagnetic activity.

1. Introduction

Adverse space weather events and disturbed ionospheric conditions may present an unfavorable environment for the operations of space-based augmentation systems (SBAS) and ground-based augmentation systems (GBAS) in aviation. In midlatitude regions, plumes of storm-enhanced density (SED) are the main source of steep ionospheric gradients that can affect the performance of SBAS/GBAS [1]. In low-latitude regions, by contrast, equatorial plasma bubbles (EPBs) are the main source [2].

In terms of risk and hazard management, there are differences in the characteristics of ionospheric threats to SBAS/GBAS in midlatitude and low-latitude regions. Threats in midlatitude regions are closely linked with severe geomagnetic storms. Although potentially posing serious effects, major geomagnetic storms do not occur very often. In the period 1958–2013, there were 1200 cases of geomagnetic storms, which statistically translates into 22 geomagnetic storms per year [3]. In another study [4], 584 geomagnetic storms were reported between 1985 and 2005, which translates into 30 geomagnetic storms per year. Among all of these, only about one-third were categorized as major geomagnetic storms. Hence, on average, at most one major geomagnetic storm may be anticipated each month, which is arguably not very often. Nevertheless, the precise timing of geomagnetic storm onset is challenging to forecast, which warrants extra caution.

In contrast, EPB occurrence exhibits a relative regularity in terms of season and time of day. As EPBs are known to be a post-sunset phenomenon, none would develop during daytime hours under quiet geomagnetic conditions. The seasonality of EPB occurrence is largely controlled by the alignment between the local magnetic meridian and the dusk terminator line. However, the day-to-day variability of EPB occurrence is still an active area of research. Hence, despite the overall regularity of EPB occurrence with season and time of day [5], its effect on the availability of SBAS/GBAS services in low-latitude regions may exceed the cumulative loss of availability in SBAS/GBAS services due to SED plumes over midlatitude regions. Hence, potential threats to SBAS/GBAS posed by EPBs also need to be carefully characterized.

Here we present an overview of our investigation into ionospheric threats to SBAS/GBAS in North and South America during solar cycle 24. Expanding on and integrating our earlier work [6–8], we characterized the loss of coverage area in the Wide Area Augmentation System (WAAS) over North America during active geomagnetic conditions, and the magnitudes of nighttime ionospheric total electron content (TEC) gradients associated with EPBs over the Brazilian airspace.

2. Data and Methodology

Both SBAS and GBAS augment the accuracy of global navigation satellite systems in civil aviation applications by using reference stations to determine position-error corrections at any given time and broadcasting these navigation corrections to aircraft. Typically, SBAS operate on a national or regional scale, whereas GBAS operate on a local scale or on the scale of airports. Figure 1 illustrates the basic operational principle of GBAS, in which navigation correction messages are broadcast by the GBAS ground facility to facilitate aircraft in runway approach and landing. Without augmentation, the horizontal and vertical position errors of GPS (at 95% confidence level) are 13 m and 22 m, respectively [11]. The augmentation provided by GBAS generally allows for precision approach with some flexibility in terms of glide path.

Manuscript received 28 December 2021.

Rezy Pradipta and Patricia Doherty are with the Institute for Scientific Research, Boston College, 140 Commonwealth Avenue, Chestnut Hill, Massachusetts 02467, USA; e-mail: rezy.pradipta@bc.edu, patricia.doherty@bc.edu.

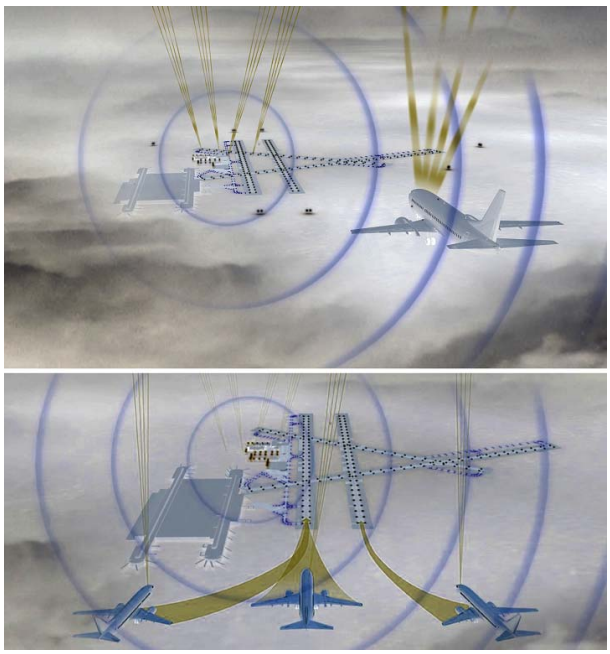

Figure 1. Conceptual illustration of GBAS operational principles. Schematic diagram adapted from [9, 10].

Steep ionospheric TEC gradients may adversely affect the accuracy of the navigation correction.

In characterizing the loss of WAAS coverage area, we used data provided by the Federal Aviation Administration (FAA)'s William J. Hughes Technical Center WAAS Test Team [12]. In those data, the total scope of the WAAS coverage area was divided into three sectors: Conterminous United States (CONUS), Canada, and Alaska. The intensity of geomagnetic storms is characterized by the disturbance storm time (Dst) index, retrieved from the Kyoto University World Data Center [13].

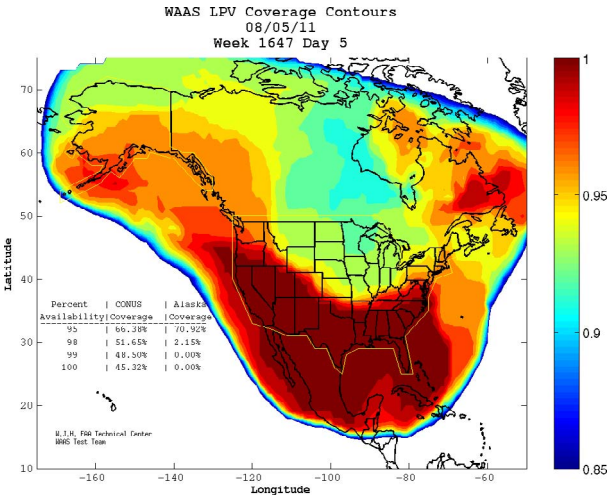

Figure 2. Example of WAAS LPV coverage-area reduction on 5 August 2011 due to a major geomagnetic storm.

In characterizing the ionospheric TEC gradient magnitudes over the Brazilian airspace, we used GPS observation data from the Brazilian Network for Continuous Monitoring of GPS (Rede Brasileira de Monitoramento Continuo dos Sistemas GNSS; RBMC), provided by the Brazilian Institute of Geography and Statistics (Instituto Brasileiro de Geografia e Estatistica; IBGE). The data were provided in RINEX file format. For the purpose of this investigation, RINEX observation data from a chain of receiver stations (BAIR, BAVC, BRAZ, CUIB, GOJA, MGMC, MTSF, MTBA, SAVO, SSA1) located along the southern crest of the equatorial ionization anomaly (EIA) region were used.

There are two ways of estimating TEC gradients, known as the station-pair method and the single-station method:

$$\nabla_{\perp}\mathrm{TEC} = \left.\frac{\mathrm{TEC}_{\mathrm{station1}} - \mathrm{TEC}_{\mathrm{station2}}}{\delta s_{12}}\right|_{\mathrm{station\ pair}} \quad (1)$$

$$\nabla_{\parallel}\mathrm{TEC} = \left.\frac{1}{v_{\mathrm{IPP}}} \cdot \frac{d\mathrm{TEC}}{dt} = \frac{d\mathrm{TEC}}{ds}\right|_{\mathrm{single\ station}} \quad (2)$$

where δs_{12} is the distance between the selected pair of stations; v_{IPP} is the velocity of the ionospheric piercing point (IPP), normally chosen at 350 km altitude; and ds is the incremental distance along the IPP trajectory. In this study, we used the single-station method to maximize the total number of samples in compiling the histograms of the TEC gradient distribution.

3. Observation Results

Figure 2 shows an example where the WAAS coverage area was significantly reduced due to disturbed geomagnetic condition. The color map indicates the percentage availability of WAAS localizer performance with vertical guidance (LPV) services during a 24 h period at each geographic coordinate point. The WAAS coverage data depicted here are from 5 August 2011, when a geomagnetic storm with a minimum Dst index of −115 nT occurred.

Within the scope of WAAS coverage, we generally found that areas closer to the auroral region are more vulnerable to reduction in LPV coverage. Nevertheless, when the geomagnetic storm is extremely intense, a massive loss of WAAS LPV coverage that affects nearly the entire CONUS region (including the southern part of the United States) can also happen.

Such an extreme case involving near-total loss of the WAAS LPV coverage happened on 25 October 2011 (data map not shown), when a major geomagnetic storm with a minimum Dst index of −147 nT occurred. On that day, the coverage area over the CONUS region (at 95% availability) dropped to 5.54%, and over the Alaska region (at 95% availability) it was 0%. Fortunately, the coverage area returned to normal the next day.

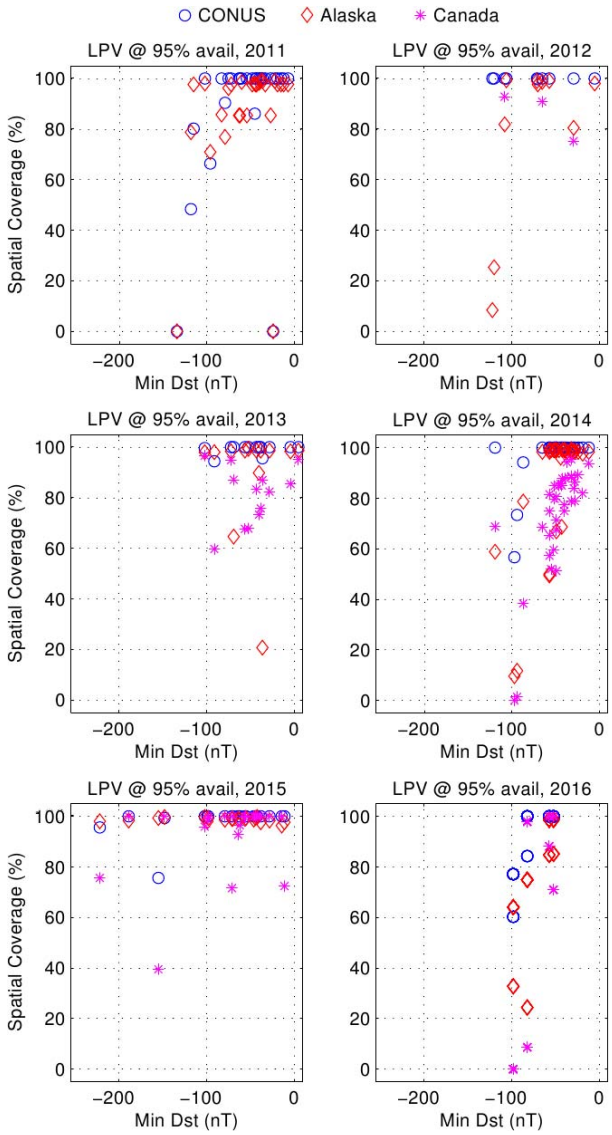

Figure 3. Reduction in WAAS LPV coverage area in 2011–2016, as a function of minimum Dst during storms.

Figure 3 shows a set of scatterplots depicting the relationship between the loss in WAAS LPV coverage area and the minimum Dst index of the corresponding geomagnetic storm. The stronger the geomagnetic storm, the more negative the associated Dst index becomes. In these scatterplots, we divided the data according to the year (2011–2016). The CONUS, Canada, and Alaska regions in each plot are represented using different symbols. Note that coverage-area data for the Canada region were only available from the year 2012 onward.

The scatterplots demonstrate a general tendency for the WAAS LPV coverage area to drop to a lower level during stronger geomagnetic storms (those with a more negative Dst index). This tendency can be seen in nearly all data panels. However, an exception can be found in the 2015 data, where a number of strong

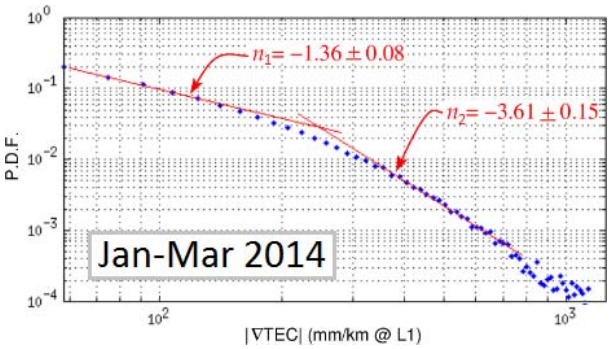

Figure 4. Example of double-power-law behavior (with exponents n_1 and n_2) found in the ionospheric TEC gradient magnitude distribution over the Brazilian airspace.

geomagnetic storms (with Dst ≤ -100 nT) did not result in much reduction of the coverage area.

Figure 4 shows the compiled histogram of EPB-related ionospheric TEC gradient magnitude distribution over the Brazilian airspace in 2014. A qualitatively similar distribution was found in other years during 2011–2016. The distribution is in the form of a double-power-law distribution, with a break point at $|\nabla \mathrm{TEC}| \approx 250$ mm/km at GPS L1 frequency and a final cutoff at $|\nabla \mathrm{TEC}| \approx 800$ mm/km. We found the exponents of this distribution to vary systematically with the sunspot number, in a way that makes the tail of the distribution extend further during the solar maximum.

Figure 5 shows the variation of the two exponents n_1 and n_2 (left vertical axis) in comparison to the variation in the sunspot number (right vertical axis). It also shows explicit least-square fits of n_1 and n_2 as a function of sunspot number (lower panel). The higher the sunspot number, the less negative these two exponents were. Consequently, the tail of the distribution would extend further during a solar maximum. By extrapolation, we may find more frequent occurrences of TEC gradients with extreme magnitudes during more active solar cycles.

4. Conclusion

In this work, we have characterized the loss of coverage area in WAAS LPV service over North America during active geomagnetic conditions, as well as the magnitudes of nighttime ionospheric TEC gradients associated with EPB occurrence over the Brazilian airspace.

We found that intense geomagnetic storms with Dst ≤ -100 nT are much more likely to cause significant reduction in the WAAS LPV coverage area, although there may be some exceptions depending on the precise storm onset time. We also found that the TEC gradient magnitudes associated with EPBs over the Brazilian airspace follow a double-power-law distribution that varies systematically following the solar cycle progression.

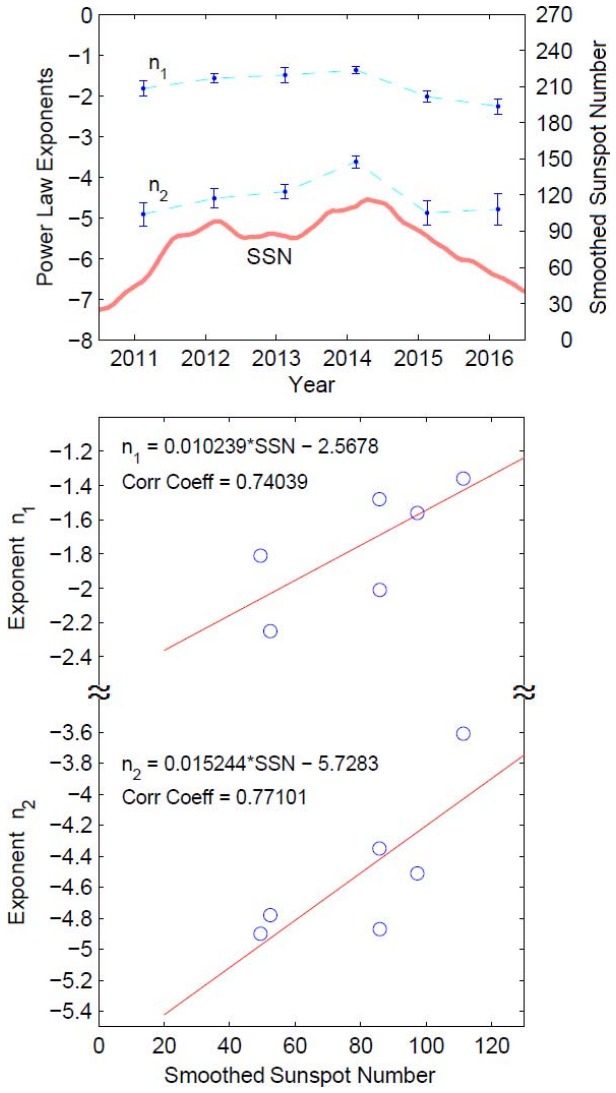

Figure 5. Systematic variation of the double-power-law exponents (n_1 and n_2) with sunspot number.

5. References

1. S. Datta-Barua, J. Lee, S. Pullen, M. Luo, A. Ene, et al., "Ionospheric Threat Parameterization for Local Area Global-Positioning-System-Based Aircraft Landing Systems," *Journal of Aircraft*, **47**, 4, July–August 2010, pp. 1141-1151.
2. M. Yoon, J. Lee, S. Pullen, J. Gillespie, N. Mathur, et al., "Equatorial Plasma Bubble Threat Parameterization to Support GBAS Operations in the Brazilian Region," *Navigation*, **64**, 3, Autumn 2017, pp. 309-321.
3. Y. Minamoto, S. Fujita, and M. Hara, "Frequency Distributions of Magnetic Storms and SI+SSC-Derived Records at Kakioka, Memambetsu, and Kanoya," *Earth, Planets and Space*, **67**, November 2015, p. 191.
4. D. Vijaya Lekshmi, N. Balan, S. Tulasi Ram, and J. Y. Liu, "Statistics of Geomagnetic Storms and Ionospheric Storms at Low and Mid Latitudes in Two Solar Cycles," *Journal of Geophysical Research: Space Physics*, **116**, A11, November 2011, p. A11328.
5. J. G. Damaceno, K. Bolmgren, J. Bruno, G. De Franceschi, C. Mitchell, et al., "GPS Loss of Lock Statistics Over Brazil During the 24th Solar Cycle," *Advances in Space Research*, **66**, 2, July 2020, pp. 219-225.
6. R. Pradipta, P. H. Doherty, R. Cole, and N. Mathur, "Observations and Analysis of the Occurrence Pattern of Large Ionospheric TEC Gradients Over the Brazilian Airspace," Proceedings of the 2016 International Technical Meeting of the Institute of Navigation, Monterey, CA, USA, January 25–28, 2016, pp. 525-531.
7. R. Pradipta and P. H. Doherty, "Assessing the Occurrence Pattern of Large Ionospheric TEC Gradients Over the Brazilian Airspace," *Navigation*, **63**, 3, Fall 2016, pp. 335-343.
8. R. Pradipta, E. Yizengaw, and P. H. Doherty, "Systematic Solar Cycle Variation of the Ionospheric TEC Gradient Magnitude Distribution Over the Brazilian Airspace," Proceedings of the 31st International Technical Meeting of the Satellite Division of the Institute of Navigation (ION GNSS+ 2018), Miami, FL, USA, September 24–28, 2018, pp. 4144-4150.
9. Honeywell Aerospace, "SmartPath Ground-Based Augmentation System," https://aerospace.honeywell.com/us/en/learn/products/sensors/smartpath-ground-based-augmentation-system (accessed 28 December 2021).
10. W. Bellamy III, "Honeywell Improves GBAS with New Software Upgrade," *Aviation Today*, https://www.aviationtoday.com/2015/11/06/honeywell-improves-gbas-with-new-software-upgrade/ (accessed 28 December 2021).
11. International Civil Aviation Organization (2006), Aeronautical Telecommunications - Annex 10 to the Convention on International Civil Aviation, Volume I (Radio Navigation Aids), Montreal: International Civil Aviation Organization.
12. "Welcome to the William J. Hughes Technical Center WAAS Test Team," https://www.nstb.tc.faa.gov/24Hr_WaasLPV.htm (accessed 1 August 2018).
13. "Geomagnetic Equatorial Dst index Home Page," http://wdc.kugi.kyoto-u.ac.jp/dstdir/ (accessed 1 August 2018).